PHYSICAL REVIEW B **78**, 140101(R) (2008)

High-pressure phases of calcium and their finite-temperature phase boundaries

A. M. Teweldeberhan and S. A. Bonev
Department of Physics, Dalhousie University, Halifax, Nova Scotia, Canada B3H 3J5
(Received 20 August 2008; published 7 October 2008)

The phase diagram of Ca up to 100 GPa and 3500 K is studied using first-principles density-functional theory. We propose two solid phases with orthorhombic *Cmcm* and *Pnma* structures and determine their finite-temperature phase boundaries. In molten Ca, we present predictions for liquid transitions under compression. Our results describe significant electronic and structural changes that are qualitatively different from those found in dense alkali liquids. The predicted liquid and solid transitions provide a consistent description of the Ca phase diagram and insight into the expected properties of other alkaline-earth metals.

DOI: 10.1103/PhysRevB.78.140101 PACS number(s): 62.50.−p, 61.20.Ja, 63.20.−e, 71.15.Mb

Substantial experimental[1–6] and theoretical[7–11] work have been devoted to study the electronic and structural properties of the high-pressure phases of Ca. Most studies to date have been carried out at room or low temperature where solid Ca undergoes transformations from close-packed to lower-symmetry structures driven by an increase in the electron *d*-band occupation (*s*-to-*d* transfer) under compression.[8,9] A major motivation for this interest are the remarkable superconducting properties of Ca. Unusually high critical temperatures of 15 K at 150 GPa (Ref. 4) and 25 K at 161 GPa (Ref. 6) were recently reported in an unknown phase. Knowledge of the structural, vibrational, and electronic properties of Ca at high pressure is required to explain this phenomenon. However, its phase diagram remains poorly understood even for pressures much below 100 GPa. At ambient conditions Ca crystallizes in the face-centered-cubic (fcc) structure. At higher pressures, Olijnyk and Holzapfel[3] reported the following structural transitions: fcc to body-centered-cubic (bcc) at 19.5 GPa, bcc to simple cubic (sc) at 32 GPa, and sc to a yet unidentified phase at 42 GPa. In accordance with Ref. 3, Dunn and Bundy[2] observed a drop in the electrical resistance of Ca at 44 GPa. However, recent experimental investigations[5,6] have not confirmed the transition at around 42 GPa and instead have proposed that the sc structure is stable in the entire 32–109 GPa pressure range.

Although the properties of solid and liquid Ca at elevated temperatures are also of significant interest, high-temperatures studies are scarce. Fundamental open questions include: (i) the realization of *s*-to-*d* transfer in the presence of ion dynamics; (ii) the persistence of low-symmetry structures, both solid and liquid, at high temperature and their electronic and structural properties; (iii) the existence of a parallel between solid and liquid transitions; and (iv) explanation for the complex shape of the measured Ca melting curve.[5]

In this Rapid Communication, we use first-principles density-functional theory to re-examine the stability of the high-pressure phases of Ca and find the sc structure to be mechanically unstable from 0 to at least 120 GPa. Instead, two orthorhombic structures with space groups *Cmcm* and *Pnma* are proposed. We have determined the finite-temperature phase boundaries between the fcc, bcc, *Cmcm*, and *Pnma* solids within the quasiharmonic approximation and present results from molecular-dynamics (MD) simulations which predict liquid transitions in compressed Ca. These results, together with available experimental data, provide a consistent description of the phase diagram of Ca up to around 100 GPa and 3500 K.

The mechanical stability and finite-temperature phase boundaries of crystalline structures were determined by calculating their phonon-dispersion relations at various pressures using density-functional perturbation theory as implemented in the ABINIT (Ref. 12) package. A pseudopotential which includes the $3p$ and $4s$ semicore states as valence states was generated with the OPIUM (Ref. 13) program. We used the generalized gradient approximation (GGA) for the exchange-correlation functional,[14] a 30 hartree plane-wave cut-off energy, and a $16\times16\times16$ Monkhorst-Pack (MP) mesh[15] for the **k**-point sampling of the Brillouin zone. For phonon-free energies, dynamical matrices were computed on a $6\times6\times6$ MP grid. Structural optimizations were carried out with the VASP code,[16,17] which employs an efficient conjugate gradient algorithm for structural relaxation. The calculations were carried out with a ten-electron projector augmented wave pseudopotential,[18,19] 14 hartree plane-wave cutoff, and the PW91 GGA parametrization.[20,21] A $12\times12\times12$ MP grid was used for ground-state self-consistent calculations and a $16\times16\times16$ one for obtaining electronic density of states (DOS). For selected pressures we verified that the same optimized structures are obtained with ABINIT and VASP.

The MD simulations were performed with VASP in a canonical (*NVT*) ensemble on systems consisting of 108 atoms in cubic supercells. The equations of motion were integrated with ionic time steps of 1 fs, the Brillouin zone was sampled at the Γ point, and the ionic temperature was controlled with a Nosé-Hoover thermostat.[22,23] Initially, liquid configurations were allowed to equilibrate for 3 ps at several pressures and temperatures well above the experimental melting curve. The simulations were then carried out for another 3 ps to gather statistical information for analyzing the liquid electronic and structural properties. Electronic DOS of the liquid configurations were calculated with a $4\times4\times4$ **k**-point mesh.

The phonon-dispersion relations along the high-symmetry points of the Brillouin zone of the sc structure at 45 GPa are shown in Fig. 1(a). The existence of soft modes (imaginary frequencies) near the *X* and *M* points indicates that this structure is mechanically unstable. We have checked the stability of the sc structure from 0 to 120 GPa and find that it is unstable in this entire pressure range. To assess the accuracy of our calculations, we have computed the phonon dispersions of the fcc structure at ambient pressure and compared

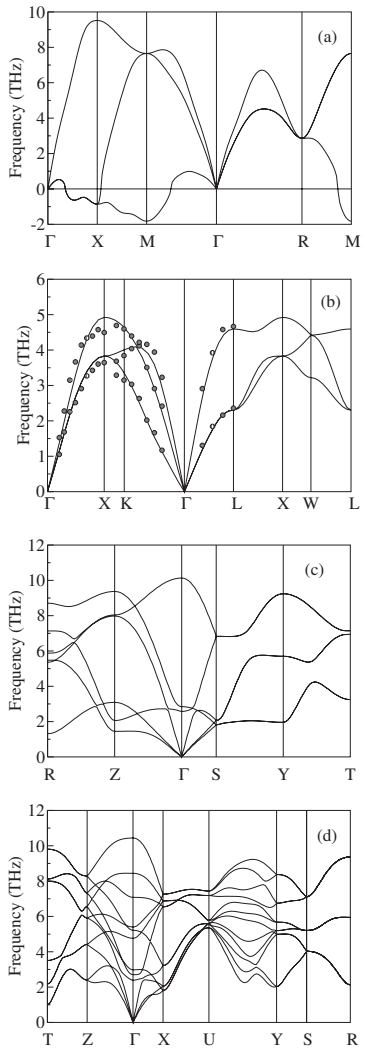

FIG. 1. Phonon-dispersion relations of Ca (a) sc at 45 GPa, (b) fcc at ambient pressure, (c) *Cmcm* at 40 GPa, and (d) *Pnma* at 50 GPa. Solid lines are calculated values and the circles in (b) are experimental data from Ref. 24.

them with available experimental data.[24] As shown in Fig. 1(b), the calculated frequencies are in excellent agreement with the experimental values (calculated and experimental equilibrium lattice constants are 5.51 and 5.58 Å, respectively). Since the calculations of sc and fcc are carried out for similar pressures and their electronic properties are also similar, we are confident about the validity of the sc phonons.

The fact that the soft modes in the sc structure are most pronounced near the high-symmetry points X and M has prompted us to use the following methodology to search for new and stable high-pressure phases. We double the sc unit cell in the x direction and slightly displace the atoms in the elongated cell according to the eigenvectors of the unstable modes. The atomic positions and supercell lattice vectors are then relaxed without symmetry restrictions to minimize enthalpy. Performing this procedure at around 40 GPa, we find a base-centered-orthorhombic (bco) structure with the *Cmcm* space-group symmetry. The phonon dispersions of *Cmcm* shown in Fig. 1(c) indicate that the structure is stable around this pressure. However, under further compression,

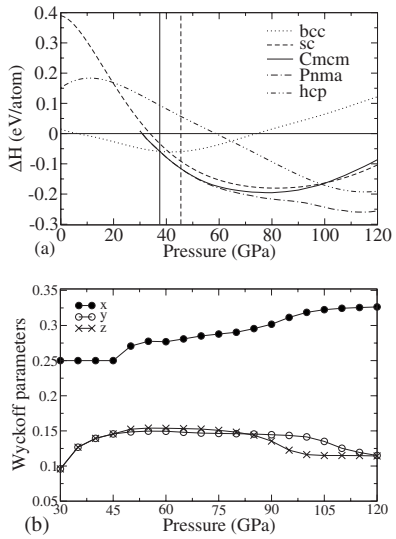

FIG. 2. (a) Enthalpies of the solid phases of Ca relative to the fcc structure. The vertical lines indicate the pressures of the bcc to *Cmcm* and *Cmcm* to *Pnma* transitions. (b) Wyckoff position parameters for the optimized *Cmcm* and *Pnma* structures as a function of pressure.

the modes near the symmetry point R begin to soften and the frequencies become imaginary above 45.5 GPa. To find the new stable phase, which must exist at pressures above 45.5 GPa, we follow a similar procedure, but we start by doubling the bco unit cell along the y and z directions. The structure obtained in this way is a simple orthorhombic with the *Pnma* space-group symmetry, and it is dynamically stable up to at least 120 GPa; *Pnma* phonons at 50 GPa are shown in Fig. 1(d).

To confirm the *thermodynamic* stability of the new structures, we have computed their enthalpies and compared them with fcc, bcc, sc, and hexagonal-close-packed (hcp). The results are shown in Fig. 2(a) for pressures from 0 to 120 GPa. According to our calculations, Ca transforms from fcc to bcc at 7 GPa, which is lower than the room-temperature experimental value of 20 GPa; see discussion about this discrepancy below. The computed transition from bcc to *Cmcm* at 37.5 GPa is close to the measurement at 32 GPa, which was previously interpreted as the bcc to sc transition. Finally, we have a *Cmcm* to *Pnma* transition at 45.5 GPa, which is in agreement with the observed phase change to an unknown structure at 42 GPa reported by Olijnyk and Holzapfel.[3] Note that *Pnma* is a maximal nonisomorphic subgroup of *Cmcm* and the phase transition between the two is martensitic. The enthalpy of the hcp structure is included in the figure because it was previously proposed by Lei *et al.*[11] as a good candidate for a high-pressure phase of Ca. However, the enthalpy of this structure remains significantly higher than that of *Pnma* even at 120 GPa.

The conventional unit cells of the new structures have four atoms per unit cell. Their Wyckoff positions are $(1/4,1/4,y)$, $(3/4,3/4,-y)$, $(1/4,3/4,y+1/2)$, and $(3/4,1/4,-y+1/2)$ for *Cmcm*; and $(-x+1/2,3/4,z+1/2)$, $(-x,3/4,-z)$, $(x,1/4,z)$, and $(x+1/2,1/4,-z+1/2)$ for *Pnma*. *Pnma* reduces to *Cmcm* when $x=1/4$. *Cmcm* can be

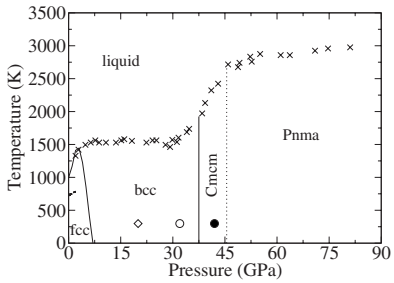

FIG. 3. Calculated phase diagram of Ca (solid and dotted lines). The crosses mark the experimental melting curve from Ref. 5 and the dashed line inside the calculated fcc-bcc phase boundary indicates the measured fcc-bcc phase transition from Ref. 1. The diamond, open, and solid circles show the experimental room-temperature phase transitions (Refs. 3, 5, and 6).

viewed as a distortion of the sc structure, and the two are equivalent when $y=-1/4$, $a/b=\sqrt{2}$, and $b=c$. With $y=0$, $a=b$, and $a/c=\sqrt{2}$ *Cmcm* becomes bcc, and with $y=0$ and $a=b=c$ it becomes fcc. The optimized values of x, y, and z as functions of pressure are plotted in Fig. 2(b). At 40 GPa, $y=0.1393$, and at 50 GPa, $x=0.2704$ and $z=0.1515$. The optimized *Cmcm* and *Pnma* have nearly sixfold coordination similar to sc but with more uniform distributions of farther neighbors.

Next, we turn our attention to the finite-temperature properties of Ca. The calculated solid phase boundaries together with available experimental data are shown in Fig. 3. They are determined by calculating the Gibbs free energy of each phase as a function of temperature for a fixed pressure and finding the points of equality between the various phases. The fcc to bcc transition temperature increases with pressure up to 3 GPa. This is in a qualitative agreement with the measured values (the dashed line) from Ref. 1. The calculated transition temperature (1000 K) at ambient pressure is in good agreement with the theoretical value (961 K) reported by Hearn *et al.*[25] but overestimates the experimental transition temperature by ~280 K. This is not surprising as the transition temperature is very sensitive to variations in free energy. A change in only 4.5 meV in the relative bcc and fcc free energies is required to obtain the experimental value (721 K). At the same time, the difference between the Gibbs free energies of bcc and fcc also decreases rapidly with pressure and becomes almost independent of temperature making it difficult to determine the room-temperature transition pressure accurately.

Near 37 GPa, the bcc and *Cmcm* phonon-free energies do not differ significantly and as a result the boundary between the two phases is almost a vertical line. It crosses the melting curve near its deflection point providing an explanation for the observed increase in its slope at higher pressure. The martensitic *Cmcm-Pnma* transition, on the other hand, has little effect on the shape of the melting curve. Its flattening below 35 GPa and above 45 GPa suggests that it is due to changes taking place in the liquid in both of these pressure ranges (possibly continuously) and/or as a function of temperature.

We have examined the liquid properties along the 2000 and 3500 K isotherms. The angle distributions among nearest

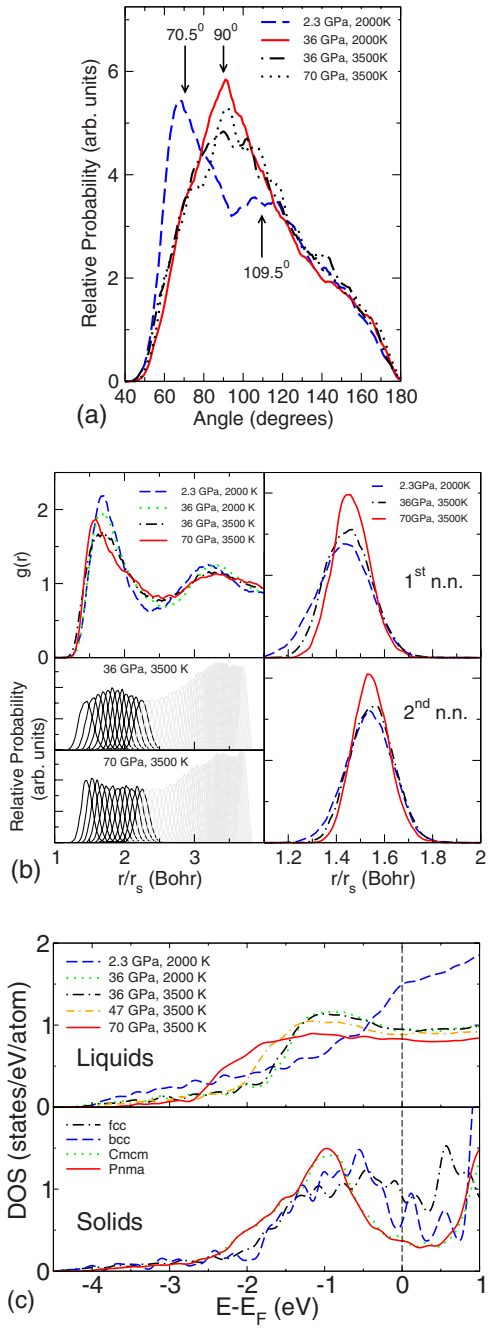

FIG. 4. (Color online) (a) Bond angle distributions between the first two neighbors in liquid Ca. The arrows indicate angles found in the ideal bcc and sc crystals. (b) Pair correlation functions and histograms of neighbor distance distributions in liquid Ca. The panels on the right show the distributions for the first and second neighbors only. (c) DOS of solid and liquid phases. All solid structure DOS are calculated at 50 GPa.

neighbors shown in Fig. 4(a) indicate that the local order of the liquid at low pressure resembles that of the underlying bcc solid. As the pressure is increased to 36 GPa, the distribution peaks near 90°. While there are some variations for angles computed between different neighbors, there is a clear distinction between distributions involving only neighbors one to six and such involving more distant neighbors. The former are close to the results shown in the figure, while the

latter exhibit well pronounced peaks between 50° and 60°. Hence, at 36 GPa the liquid develops an octahedral local order, which is favored by the valence electrons developing a (partial) *d*-bonding character. This conclusion is supported by the observed changes in electronic DOS [Fig. 4(c)]; there is a shift in the DOS from around the Fermi level to lower energies, similar to what happens in the solid upon transition to *Cmcm* and *Pnma*. The *s*-to-*d* charge transfer lowers the band-structure energy of the liquid thus increasing its compressibility, which explains the flattening of the melting curve up to 36 GPa.

At higher pressures, the angular distributions do not change significantly. Additionally, in contrast to liquid Li (Ref. 26) and Na (Ref. 27) where *s*-to–*p* transfer leads to a decrease in the coordination number, in Ca it remains unchanged from 0 up to at least 70 GPa. The most pronounced change in the pair correlation function [Fig. 4(b)] is the sharpening of its first peak, which begins to develop above 40 GPa. For a more detailed analysis, we compute histograms of neighbor distances. When rescaled by density, the average positions of these distance distributions do not change noticeably with pressure. However, as shown in the bottom left panel of Fig. 4(b), the profiles of the first ~6 curves *do change*. The curves for the first and second neighbors plotted on the right show that the spread of the distances over which each of the first few neighbors can be found decreasing with pressure. The implication is that the correlation among atoms in octahedral coordination increases, and there are "preferred" distances at which they tend to localize. This is consistent with the observed shift in the DOS to lower values below E_F and the decrease in valence bandwidth between 36 and 70 GPa. The consequences are again increased compressibility of the liquid and flattening of the melting curve above 40 GPa.

In summary, we proposed two crystal structures for Ca, *Cmcm*, and *Pnma* and computed the finite-temperature boundaries of all solid phases found below 120 GPa. We predicted electronic and structural transitions in liquid Ca in the range from 0 to 70 GPa and 2000 to 3500 K. These changes can be understood in terms of *s* to *d* charge transfer and development of octahedral local order in the liquid. As in Li and Na,[26,27] there is a clear analogy between the changes found in solid and liquid Ca, and these transitions provide explanation for the observed melting curve shape. However, in the case of Ca, they are insufficient for producing anomalous melting; at least in the pressure range considered here. The computed DOS suggest that the liquid transitions should be accompanied by a substantial decrease in electrical conductivity, an effect which might be measurable. Further theoretical investigations of the superconducting properties of the proposed structures may also be of interest; for the sc structure, Lei *et al.*[11] found the superconducting transition temperature to be much higher than the experimental value. Finally, we propose Raman or neutron-scattering measurements for experimental confirmation of the *Cmcm* and *Pnma* structures. Although Raman measurements of simple metals are not straightforward, they have been used successfully to study simple metals under pressure.[28] *Cmcm* has A_g and B_{1g} Raman-active modes with frequencies 2.58 and 10.13 THz, respectively, at 40 GPa, while *Pnma* has $2A_g$, B_{2g}, B_{3g}, and B_{1g} modes with frequencies 2.39, 2.71, 4.76, 5.21, and 8.44 THz, respectively, at 50 GPa.

This work was supported by NSERC and ACEnet. The authors would like to thank ACEnet, SHARCNET, WestGrid, and LLNL for providing computational facilities.

[1] A. Jayaraman, W. Klement, Jr., and G. C. Kennedy, Phys. Rev. **132**, 1620 (1963).
[2] K. J. Dunn and F. P. Bundy, Phys. Rev. B **24**, 1643 (1981).
[3] H. Olijnyk and W. B. Holzapfel, Phys. Lett. **100A**, 191 (1984).
[4] S. Okada, K. Shimizu, T. Kobayashi, K. Amaya, and S. Endo, J. Phys. Soc. Jpn. **65**, 1924 (1996).
[5] D. Errandonea, R. Boehler, and M. Ross, Phys. Rev. B **65**, 012108 (2001).
[6] T. Yabuuchi, T. Matsuoka, Y. Nakamoto, and K. Shimizu, J. Phys. Soc. Jpn. **75**, 083703 (2006).
[7] J. A. Moriarty, Phys. Rev. B **8**, 1338 (1973).
[8] H. L. Skriver, Phys. Rev. Lett. **49**, 1768 (1982).
[9] R. Ahuja, O. Eriksson, J. M. Wills, and B. Johansson, Phys. Rev. Lett. **75**, 3473 (1995).
[10] G. M. Wang, D. A. Papaconstantopoulos, and E. Blaisten-Barojas, J. Phys. Chem. Solids **64**, 185 (2003).
[11] S. Lei, D. A. Papaconstantopoulos, and M. J. Mehl, Phys. Rev. B **75**, 024512 (2007).
[12] X. Gonze, J.-M. Beuken, R. Caracas, F. Detraux, M. Fuchs, G.-M. Rignanese, L. Sindic, M. Verstraete, G. Zerah, F. Jollet, M. Torrent, A. Roy, M. Mikami, Ph. Ghosez, J.-Y. Raty, and D. C. Allan, Comput. Mater. Sci. **25**, 478 (2002).
[13] A. M. Rappe, K. M. Rabe, E. Kaxiras, and J. D. Joannopoulos, Phys. Rev. B **41**, 1227 (1990).
[14] J. P. Perdew, K. Burke, and M. Ernzerhof, Phys. Rev. Lett. **77**, 3865 (1996).
[15] H. J. Monkhorst and J. D. Pack, Phys. Rev. B **13**, 5188 (1976).
[16] G. Kresse and J. Hafner, Phys. Rev. B **47**, 558 (1993).
[17] G. Kresse and J. Furthmüller, Phys. Rev. B **54**, 11169 (1996).
[18] P. E. Blöchl, Phys. Rev. B **50**, 17953 (1994).
[19] G. Kresse and D. Joubert, Phys. Rev. B **59**, 1758 (1999).
[20] Y. Wang and J. P. Perdew, Phys. Rev. B **44**, 13298 (1991).
[21] J. P. Perdew, J. A. Chevary, S. H. Vosko, K. A. Jackson, M. R. Pederson, D. J. Singh, and C. Fiolhais, Phys. Rev. B **46**, 6671 (1992).
[22] S. Nosé, J. Chem. Phys. **81**, 511 (1984).
[23] W. G. Hoover, Phys. Rev. A **31**, 1695 (1985).
[24] C. Stassis, J. Zaretsky, D. K. Misemer, H. L. Skriver, B. N. Harmon, and R. M. Nicklow, Phys. Rev. B **27**, 3303 (1983).
[25] J. E. Hearn, R. L. Johnston, S. Leoni, and J. N. Murrell, J. Chem. Soc., Faraday Trans. **92**, 425 (1996).
[26] I. Tamblyn, J.-Y. Raty, and S. A. Bonev, Phys. Rev. Lett. **101**, 075703 (2008).
[27] J.-Y. Raty, E. Schwegler, and S. A. Bonev, Nature (London) **449**, 448 (2007).
[28] A. F. Goncharov, V. V. Struzhkin, H. K. Mao, and R. J. Hemley, Phys. Rev. B **71**, 184114 (2005).